

Molecular dynamics simulations of critically percolated, cluster-packed structure in Zr–Al–Ni bulk metallic glass

A. Takeuchi · K. Yubuta · M. Ogata ·

A. Inoue

Received: 27 September 2009 / Accepted: 22 February 2010 / Published online: 9 March 2010
© Springer Science+Business Media, LLC 2010

Abstract We have studied the local atomic arrangements of a $Zr_{0.60}Al_{0.15}Ni_{0.25}$ bulk metallic glass (BMG) with molecular dynamics (MD) simulations based on a plastic crystal model (PCM). We have utilized features of orientationally disordered state of a molecule in plastic crystals. A $Zr_{0.618}Al_{0.146}Ni_{0.236}$ alloy with an approximated composition to the $Zr_{0.60}Al_{0.15}Ni_{0.25}$ has been created using MD–PCM from a $Zr_{0.73}Ni_{0.27}$ glassy alloy that possesses critically percolated Ni atoms. The MD–PCM dealt with icosahedral and tetrahedral clusters with 13 and five atoms, respectively, with a Ni, Al, or Zr atom at each center site of the clusters. After the $Zr_{0.73}Ni_{0.27}$ glassy alloy had been created with monatomic MD simulation by quenching from a liquid, the Zr and Ni atoms in the $Zr_{0.73}Ni_{0.27}$ glassy alloy were replaced with randomly oriented icosahedral and tetrahedral clusters, respectively. Subsequently, structural relaxation was performed after adjusting the density to that of the $Zr_{0.618}Al_{0.146}Ni_{0.236}$ alloy. Total pair-distribution and interference functions revealed that the $Zr_{0.618}Al_{0.146}Ni_{0.236}$ alloys created with MD–PCM exhibit the characteristics of a non-crystalline phase. Further, Voronoi polyhedra analysis revealed that the Ni-centered polyhedral clusters used as initial atomic arrangements for MD–PCM tend to

reproduce the features of the conventional MD results. The origin of the excellent glass-forming ability of the $Zr_{0.618}Al_{0.146}Ni_{0.236}$ alloy is attributed to the critically percolated cluster-packed structure.

Introduction

Recently, many bulk metallic glasses (BMGs) have been fabricated in binary and multicomponent metallic systems with a transition metal (TM) as the main constituent [1–8]. For instance, one can list Zr- and Cu-based BMGs that include Ni, Al, and other constituents simultaneously or separately as the TM-base BMGs. Specifically, the binary BMGs contain Cu–Zr [1–3] alloys whereas the multicomponent [7, 8] BMGs include Zr–Al–(Cu, Ni) base alloys [4–7]. The binary BMGs provide great advantage over the multi-component BMGs for theoretical and computational analysis because of the small number of constituent elements and their atomic pairs. However, the disadvantage of binary BMGs over the multi-component BMGs is the lower maximum sample dimensions, which relate to the glass-forming ability (GFA). Specifically, the critical dimensions (d_c) for forming a single glassy phase in binary BMGs are a few millimeters or less [1–3], whereas those in multi-component BMGs exceed a few centimeters [7, 8]. The significant difference in d_c between binary and multi-component BMGs suggests that the local atomic arrangements change drastically with multi-component alloying. Hence, we should pay attention to the ternary alloy systems to analyze the origin of high GFA by taking into account the common features underlying binary and multi-component BMGs.

As a prototype for the Zr-based multi-component BMGs, one can consider a $Zr_{0.60}Al_{0.15}Ni_{0.25}$ ternary BMG

A. Takeuchi (✉) · A. Inoue
World Premier International Research Center,
Tohoku University, Sendai, Japan
e-mail: takeuchi@wpi-aimr.tohoku.ac.jp

K. Yubuta
Institute for Materials Research, Tohoku University, Sendai,
Japan

M. Ogata
Graduate School of Engineering, Tohoku University, Sendai,
Japan

[4], which is similar to the Cu_{0.618}Zr_{0.382} binary BMG since they contain a composition ratio equal to the golden mean ($\phi \sim 1.618$). Specifically, we have reported [9] that the Cu_{0.618}Zr_{0.382} and Zr_{0.60}Al_{0.15}Ni_{0.25} BMGs can be approximated as Cu _{ϕ^{-1}} Zr _{ϕ^{-2}} and Zr _{ϕ^{-1}} Al _{ϕ^{-4}} Ni _{ϕ^{-3}} (\sim Zr_{0.618}Al_{0.146}Ni_{0.236}), respectively. A further analysis of the golden mean composition alloy predicts the ability of the BMG to have packed clusters of icosahedra and tetrahedra. The ideal ratio of the number density of the icosahedral and tetrahedral clusters is $\phi^2:1$ [9]. The presence of icosahedral and tetrahedral clusters here has been supported by three early studies [10–12]. For instance, Finney and Wallage [10] have reported that local units such as icosahedra can be unambiguously identified in terms of clusters of distorted tetrahedral, whereas Fang et al. [11] performed ab initio molecular dynamics (MD) simulations for pure Zr [11], indicating that the short range order in liquid and glassy states is mostly due to icosahedral, tetrahedral, and bcc clusters. As for alloys, Kelton et al. [12] have reported that the icosahedral configuration increases with undercooling in Ti_{39.5}Zr_{39.5}Ni₂₁ liquid. However, they also found that the icosahedral short range order was distorted, likely becoming more tetrahedral and possibly developing a crystallographic-type local order. The ratio of icosahedral and tetrahedral clusters, $\phi^2:1$, [9] yields the fraction of tetrahedral clusters of 0.276, and that this value is near the critical concentration of site percolation (p_c^{site}) ~ 0.27 for the dense random packing (DRP) structure [13, 14]. In order to validate this prediction, we have performed MD simulations for the Cu_{0.618}Zr_{0.382} BMG [15]. In these simulations, we have used a plastic crystal model (PCM), which involves random rotations of clusters and subsequent structural relaxations. The results of MD–PCM for the Cu_{0.618}Zr_{0.382} BMG revealed formation of the noncrystalline alloy, as well as the roles of the distorted tetrahedral clusters in forming a network within a DRP structure. It is thus worth extending the computational analyses with MD–PCM to the Zr_{0.60}Al_{0.15}Ni_{0.25} BMG, which has a larger GFA.

The present study aims to perform MD–PCM for the typical Zr_{0.618}Al_{0.146}Ni_{0.236} BMG, and to analyze the reason for the high GFA of the Zr_{0.60}Al_{0.15}Ni_{0.25} BMG.

Method

Alloys, clusters, and assignments of atoms in clusters

Two kinds of alloys were simulated in the present study: a Zr_{0.618}Al_{0.146}Ni_{0.236} (\sim Zr _{ϕ^{-1}} Al _{ϕ^{-4}} Ni _{ϕ^{-3}}) alloy with a composition close to that of Zr_{0.60}Al_{0.15}Ni_{0.25} BMG and a Zr_{0.73}Ni_{0.27} alloy. Here, the Zr_{0.73}Ni_{0.27} alloy was tentatively modeled in the process of modeling the

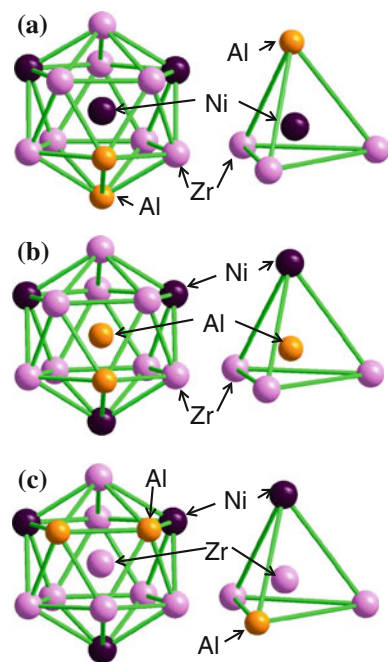


Fig. 1 Ball and stick views for icosahedral and tetrahedral clusters with 13 and five atoms, respectively, where the atom at the center site is **a** Ni, **b** Al, and **c** Zr. The icosahedron comprises eight Zr, two Al, and three Ni atoms while the tetrahedral cluster consists of three Zr, one Al, and one Ni atoms. The edge length is determined to be 0.320 nm ($= 2r_{\text{Zr}}$), leading to the ratio of the greatest circumradii (r_{circum}) from the center site (r_{circum} for polyhedra comprising vertices plus r_{Zr}) of the polyhedra being close to the ratio of $r_{\text{Zr}}/r_{\text{Ni}}$. See Table 2 for details

Zr_{0.618}Al_{0.146}Ni_{0.236} alloy, due to the former having local atomic arrangements with p_c^{site} of 0.27 in the three-dimensional structure for DRP [13, 14]. More precisely, the Zr_{0.618}Al_{0.146}Ni_{0.236} alloy was created by exchanging the icosahedral and tetrahedral clusters with Zr and Ni atoms of the Zr_{0.73}Ni_{0.27} alloy, respectively. Figure 1 shows the icosahedral and octahedral clusters comprising Zr, Al, and Ni atoms, shown as balls and sticks. Figure 1a–c illustrates the three possible types of polyhedra (icosahedron and tetrahedron), where either Ni, Al, or Zr atoms occupy the center sites of each polyhedron. The icosahedral cluster has 13 atoms—eight Zr, two Al, and three Ni atoms, whereas the octahedral cluster possesses five atoms—three Zr, one Al, and one Ni. We have determined that here the atomic radii of Zr, Al, and Ni (r_{Zr} , r_{Al} , and r_{Ni}) are 0.160, 0.143, and 0.125 nm [16], respectively, and the edge lengths of the polyhedra are $2r_{\text{Zr}}$. This implies that the ratio of the specific lengths of the polyhedra, such as the polyhedra radii being close $r_{\text{Zr}}/r_{\text{Ni}}$. This close ratio allows us to tentatively use the Zr_{0.73}Ni_{0.27} alloy in the process of creating the Zr_{0.618}Al_{0.146}Ni_{0.236} alloy, by substituting the Zr and Ni atoms in the binary alloy with the polyhedra. The substitutions of the atoms with the clusters and vice versa arise from the widely accepted concept of a renormalization

Table 1 The topological features [14] of icosahedral and tetrahedral polyhedra and clusters used in the present study

	Icosahedron	Tetrahedron
Faces	20	6
Edges	30	6
Vertices	12	4
No. atoms	13	5
Interatomic distance: (edge)	$2r_{\text{Zr}} (=a)$	$2r_{\text{Zr}} (=a)$
Circumradius of polyhedron	$\sqrt{\frac{5+\sqrt{5}}{8}}a \sim 0.951a$	$\frac{\sqrt{6}}{4}a \sim 0.613a$
Greatest circumradius of clusters	$\sqrt{\frac{5+\sqrt{5}}{8}}a + r_{\text{Zr}}$ $\sim 2.902r_{\text{Zr}}$	$\frac{\sqrt{6}}{4}a + r_{\text{Zr}}$ $\sim 2.226r_{\text{Zr}}$

The circumradius and the greatest circumradius for the polyhedra including atoms at vertices were calculated on the basis of the edge length (a) using atomic radius of Zr atom (r_{Zr}). The ratio of the greatest circumradii between the icosahedral and tetrahedral clusters are evaluated to be 1.30 (2.902/2.226), which is close to those of the atomic radii of 1.28 ($= r_{\text{Zr}}/r_{\text{Ni}}$) [13] between Zr and Ni atoms

group in statistical mechanics. The details of the polyhedra lengths determinations are summarized in Table 1, in which the set of fundamental topologies of polyhedra has been acquired from the literature [17]. In Fig. 1, we have placed the coordination atoms by considering the symmetry of each polyhedron to be allowed. Figures 1a, b differ from Fig. 1c because in them solute atoms (Ni and Al) occupy the center sites of the polyhedra. Placing solute atoms in a cluster agrees with the recent models proposed by Miracle [18, 19] and Sheng et al. [20], both of which have the ability to deal with medium-range order in a DRP. The coordination atoms in Fig. 1 do not show complete symmetry in space due to the limitations of the number of atoms being integers. However, it is possible that the random rotations of clusters around the center of gravity in MD–PCM will compensate for the lack of completeness of the symmetry due to the asymmetry of solute elements in each polyhedron. The density, ρ , of the $\text{Zr}_{0.73}\text{Ni}_{0.27}$ and $\text{Zr}_{0.618}\text{Al}_{0.146}\text{Ni}_{0.236}$ alloys was calculated to be 7.254 and 6.53 Mg/m^3 , respectively, from the literature [21].

Molecular dynamics (MD) simulations and analyses

Molecular dynamics (MD) simulations were performed with commercial software (Fujitsu, Materials Explorer Ver. 5) based on the PCM [22]. MD–PCM utilizes the positional order and orientational disorder features of plastic crystals [23, 24]. In our previous studies, MD–PCM has been applied to C_6Cr_{23} [25], metastable Zr_2Ni [26] structures and others to analyze their GFA, among other features. The main features of MD–PCM are summarized in the following four points:

- (1) A non-crystalline structure in a glassy phase is related to a corresponding crystalline structure, which is usually determined by referring to experimental results and considering crystallographic features.
- (2) In the corresponding crystalline structure, we assume the presence of hypothetical clusters.
- (3) We then allow the random rotations of clusters around the center of gravity around each cluster.
- (4) Finally, structural relaxation or annealing at low temperature is applied to the system.

Utilizing these four steps, we aim to extend the applicability of the MD–PCM.

In order to extend MD–PCM we introduce the concept of quenching from a melt to form a glassy structure. This is equivalent to introducing a time–temperature–transition (T–T–T) diagram in the literature [27]. The schematic T–T–T diagram illustrates that the cluster-like atomic arrangements in liquid metals can be under-cooled well below their melting temperature. When followed by the freezing-in of the under-cooled liquid at the glass transition temperature, T_g , this results in the glassy structure. The roles of cluster rotation in an extended MD–PCM in the present study are to create disorder in cluster orientation, which may exist in a liquid phase at a certain time, and to let the alloy freeze into a solid by quenching. The actual MD–PCM techniques in the present study are identical to those in our previous study for the $\text{Cu}_{0.618}\text{Zr}_{0.382}$ alloy [15]. Specifically, the $\text{Zr}_{0.618}\text{Al}_{0.146}\text{Ni}_{0.236}$ alloy was created in the following two steps: rapid quenching and subsequent annealing that correspond to α and β relaxations [28, 29] of glassy materials, respectively. First, the $\text{Zr}_{0.73}\text{Ni}_{0.27}$ glassy alloy comprising 125 atoms with $\rho = 7.254 \text{ Mg/m}^3$ was created by a conventional MD simulation through a quenching process from 2500 to 500 K. The MD simulation conditions contain a universal force field (UFF) potential, the number of atoms, temperature, and volume (constant-NTV) ensemble, and periodic boundary conditions. The $\text{Zr}_{0.618}\text{Al}_{0.146}\text{Ni}_{0.236}$ alloy comprising 1353 atoms with $\rho = 6.53 \text{ Mg/m}^3$ was created from the $\text{Zr}_{0.73}\text{Ni}_{0.27}$ glassy alloy through MD–PCM under a generalized embedded atom method (GEAM) potential. Further, structural relaxation was applied at 100 K for 1 ps. In addition to the MD–PCM, conventional monatomic MD simulations were also performed for the $\text{Zr}_{0.618}\text{Al}_{0.146}\text{Ni}_{0.236}$ alloy of 1353 atoms with $\rho = 6.53 \text{ Mg/m}^3$ under GEAM potential, as well as periodic boundary conditions and number of atoms, temperature, and pressure (constant-NTP) ensemble. The conventional MD simulation procedure includes quenching from a liquid: holding at 2100 K for 1 ps, followed by quenching from 2100 K to 100 K at a cooling rate of 10^{15} K/s for 2 ps and further structural relaxation at 100 K for 1 ps. The MD–PCM and conventional MD conditions are summarized in Table 2.

Table 2 The simulation conditions for MD-PCM and conventional monatomic MD simulation and experimental data

Step/alloy symbol	Alloy	No. atoms	Method	Status	Components	MD potential	Treatment	Ref
Step 1	Zr _{0.73} Ni _{0.27}	125			Atoms	UFF	^a Quench	—
Step 2/I	Zr _{0.618} Al _{0.146} Ni _{0.236}	1353	MD-PCM	—	Clusters	GEAM	^b Struc. Relax.	—
Step 2/II	Zr _{0.618} Al _{0.146} Ni _{0.236}	1353	MD-PCM	—	Clusters	GEAM	^b Struc. Relax.	—
Step 2/III	Zr _{0.618} Al _{0.146} Ni _{0.236}	1353	MD-PCM	—	Clusters	GEAM	^b Struc. Relax.	—
IV	Zr _{0.618} Al _{0.146} Ni _{0.236}	1353	MD	As-Q.	Atoms	GEAM	^c Quench	—
V	Zr _{0.618} Al _{0.146} Ni _{0.236}	1353	MD	Relax.	Atoms	GEAM	^c Quench + ^b Struc. Relax.	—
VI	Zr _{0.6} Al _{0.15} Ni _{0.25}	—	Experiment	As-Q.	—	—	—	[21]
VII	Zr _{0.6} Al _{0.15} Ni _{0.25}	—	Experiment	S.C.L.	—	—	—	[21]

As-Q. as-quenched state, S.C.L. supercooled liquid state

^a Quench: holding at 2500 K for 1 ps, followed by quenching at a rate of 10^{15} K s⁻¹, from 2500 to 500 K

^b Structural relaxation: 100 K, 1 ps

^c Quench: holding at 2100 K for 1 ps, followed by quenching at a rate of 10^{15} K s⁻¹, from 2100 to 100 K

The alloys created with MD-PCM and conventional MD simulations were analyzed with Voronoi polyhedra, as well as total pair-distribution and interference functions. The latter two were calculated using commercial software, whereas Voronoi analysis was carried out with a homebuilt program.

Results and discussion

Figure 2a shows atomic arrangements of the Zr_{0.73}Ni_{0.27} glassy alloy created by conventional monatomic MD simulations from a liquid in step 1. It appears that the Zr_{0.73}Ni_{0.27} alloy loses long-range periodicity intrinsic to a crystalline phase. The structure was investigated via its total pair-distribution function, $g_{\text{total}}(r)$, as shown in Fig. 2b. This figure indicates that the alloy was formed in a

non-crystalline or glassy structure, since $g_{\text{total}}(r)$ profile exhibits rather broad first and second peaks around $r = 0.27$ and 0.5 nm, respectively, approaching a value of unity for higher r . The ability of Ni atoms to percolate in the Zr_{0.73}Ni_{0.27} glassy alloy is investigated and shown in Fig. 2c. Here, the lines connecting Ni atoms in Fig. 2c show the correlations of the Ni atoms, placed at a nearest neighbor distance of 0.2–0.4 nm of Fig. 2b. Ideally, these lines should penetrate the system in the MD simulation, since the Zr_{0.73}Ni_{0.27} alloy created by atomistic MD through quenching from a liquid is expected to show a DRP structure with $p_c^{\text{site}} = 0.27$. In reality, Fig. 2c shows that not all the lines penetrate the system. However, Fig. 2b shows some degree of Ni atom percolation. Accordingly, we conclude that the Zr_{0.73}Ni_{0.27} alloy was formed in a close phase of DRP with critically percolated Ni atoms.

The Zr_{0.618}Al_{0.146}Ni_{0.236} alloy was then created with MD-PCM in step 2. Figure 3a, b shows atomic arrangements of the Zr_{0.618}Al_{0.146}Ni_{0.236} alloys created by MD-PCM using polyhedra as shown in Fig. 1a. Figure 3a replaces the Zr and Ni atoms of Fig. 2a with the randomly oriented icosahedral and tetrahedral clusters around each center of gravity. After MD-PCM, the local atomic structure shown in Fig. 3b demonstrates the randomly distributed atomic arrangements, which are different from regular atomic arrangements inherent in a crystalline structure. The atomic displacements during structural relaxations were approximately half of the interatomic distances, in agreement with our previous studies [9, 15]. Thus, distortions of polyhedra were achieved during structural relaxation, which would change the feature of short range order intrinsic to the center site and vertex atoms. In order to examine the local atomic arrangements of the alloy created with MD-PCM, total pair-distribution functions were calculated for the alloys.

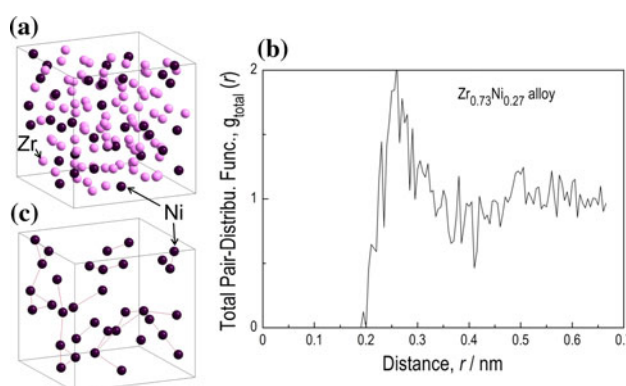


Fig. 2 Simulation results for the Zr_{0.73}Ni_{0.27} alloy. **a, c** Ball and stick views of the atomic arrangements of the Zr_{0.73}Ni_{0.27} alloy and those of the Ni components, respectively. **b** The total pair-distribution function, $g_{\text{total}}(r)$. The lines connecting Ni atoms in **c** show the correlations of the Ni atoms, placed at a nearest neighbor distance of 0.2–0.4 nm of **b**

Fig. 3 Ball and stick views for arrangements of components (atoms and clusters) for the $Zr_{0.618}Al_{0.146}Ni_{0.236}$ alloy **a** before and **b** after the structural relaxations

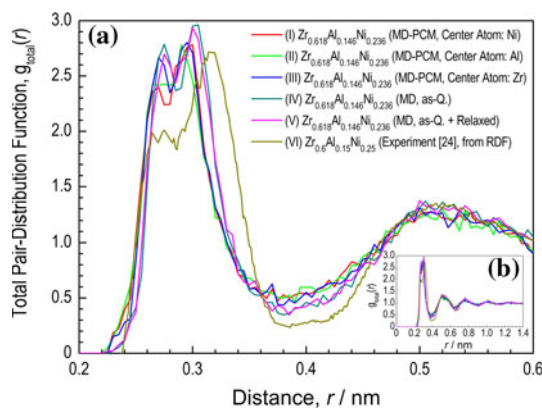
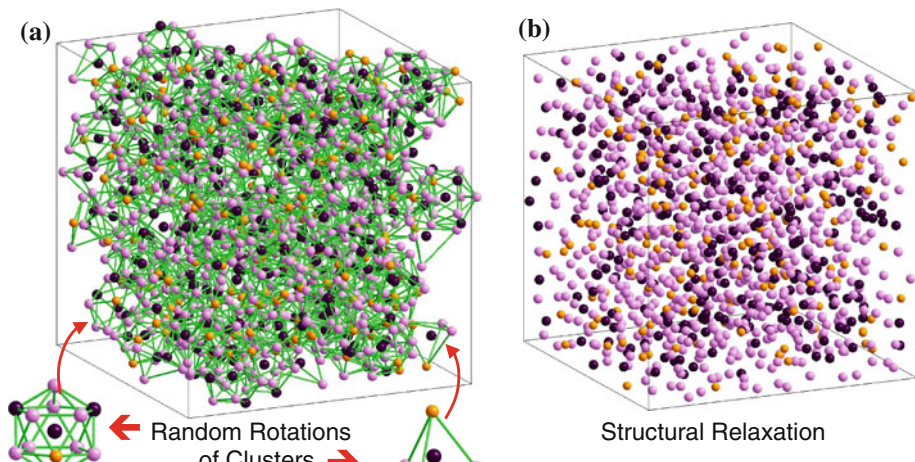


Fig. 4 The total pair-distribution function, $g_{\text{total}}(r)$, of the $Zr_{0.618}Al_{0.146}Ni_{0.236}$ alloys simulated in the present study (profiles I–V), and an experimental data [20] converted from the radial distribution function. Profiles I–III were calculated for the $Zr_{0.618}Al_{0.146}Ni_{0.236}$ alloys by MD–PCM for different types of clusters which are characterized by the center atom corresponding to Fig. 1a–c, respectively. Profiles IV and V were results from conventional MD simulations, either as-quenched or after further structural relaxation

Figure 4 shows the calculated values of $g_{\text{total}}(r)$ for the $Zr_{0.618}Al_{0.146}Ni_{0.236}$ alloys created with MD–PCM (I–III) and with conventional MD simulations in an as-quenched (IV) and further relaxed (V) states. In addition, the $g_{\text{total}}(r)$ profile for the $Zr_{0.60}Al_{0.15}Ni_{0.25}$ alloy obtained experimentally from a radial distribution function (RDF) [30] is shown in Fig. 4 as profile VI for comparison. Figure 4b shows the values of $g_{\text{total}}(r)$ for r ranging from 0 to 1.4 nm, indicating that $g_{\text{total}}(r)$ profiles (I)–(VI) sharply increase near $r = 0.2$ nm and show maximum peaks at r ranging from 0.27 to 0.31 nm, followed by converging variation in $g_{\text{total}}(r)$ with sub-peaks in the range of $r \geq 0.4$ nm. The value of the $g_{\text{total}}(r)$ at $r = 1.4$ nm reaches unity, indicating that liquid-like structures formed for the results shown in profiles I–V. In the experimental data—profile VI in Fig. 4a—the first peak at r between 0.27 and 0.31 nm has

an asymmetric shape due to a rather small shoulder at $r \sim 0.27$ nm. A similar shoulder occurs for each first peak for profiles I–V obtained computationally, although the relative intensities of the shoulder and the first peak are different. Figure 4 demonstrates that the results obtained with MD–PCM exhibit the same trends as those from conventional MD.

Further analysis using an interference function, $Qi(Q)$, was performed for the $Zr_{0.618}Al_{0.146}Ni_{0.236}$ alloy created with MD–PCM and conventional monatomic MD simulations. The results were compared with the experimental data for the $Zr_{0.60}Al_{0.15}Ni_{0.25}$ alloy from a literature [22]. As shown in Fig. 5, the $Qi(Q)$ profiles are similar for Q ranging from 0 to 60 nm^{-1} but differ for $Q > 60 \text{ nm}^{-1}$. The difference in $Qi(Q)$ profiles for high Q greater than 60 nm^{-1} is presumably due to the oversimplifying assumptions of MD–PCM compared to those of

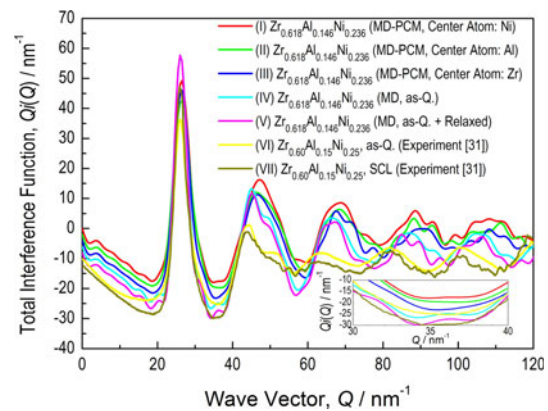


Fig. 5 The total interference function, $Qi(Q)$, plotted with a vertical interval of 2 nm^{-1} for $Qi(Q)$ to avoid overlap. Profiles I–III are obtained from MD–PCM, profiles IV–V come from conventional MD, and profiles V–VI are the experimentally measured data [31] for the $Zr_{0.60}Al_{0.15}Ni_{0.25}$ alloys in an as-quenched and supercooled liquid region, respectively. Profiles I–III correspond to simulation results obtained using clusters for Fig. 1a–c, respectively

conventional MD and the experiments. Thus, we do not discuss the details of the disagreement of $Qi(Q)$ profiles at high $Q > 60 \text{ nm}^{-1}$, since this is outside the scope of the present study. For $Q \leq 60 \text{ nm}^{-1}$, $Qi(Q)$ profiles in Fig. 5 show the following three tendencies. First, profiles I–III show the sharp primary peak around $Q \sim 26 \text{ nm}^{-1}$. The presence of the primary peaks around $Q \sim 26 \text{ nm}^{-1}$ agrees with the experimental data of an as-quenched state and supercooled liquid state (SCL) [31] shown as profiles VI and VII as well as the conventional MD results shown as profiles IV–V. Second, there is a shoulder around $Q \sim 45\text{--}50 \text{ nm}^{-1}$ only for profiles IV–VI. The lack of the shoulder peak around $Q \sim 45\text{--}50 \text{ nm}^{-1}$ for other profiles suggests that the alloys created with MD–PCM in the present study are formed in liquid-like states rather than amorphous solid-like structure. However, profile I has a rather weak inflection point around $Q \sim 50 \text{ nm}^{-1}$. Third, there is a small difference in the shape of profiles around $Q \sim 36 \text{ nm}^{-1}$, which are shown in the inset in Fig. 5, although the profiles I to III show no significant differences at Q ranging from 0 to 65 nm^{-1} . In the inset, the profiles I–III around $Q \sim 36 \text{ nm}^{-1}$ change their $Qi(Q)$ from a “W”-shape for profile I to a “U”-shape for profile III. The “W”-shape of $Qi(Q)$ is also seen in the inset for profiles IV–V created with conventional MD simulations, indicating that profile I gives the best agreement with the results obtained by conventional MD simulations.

The above three trends indicate that the alloys created with MD–PCM in the present study are formed in liquid-like states. Profile I is best at reproducing the results obtained by conventional MD simulations among the MD–PCM profiles. The reason for this is presumably due to the topological fitness to form polyhedra with 13 atoms when Ni being a smaller atom, rather than Zr or Al, is located at the center site. For instance, it is widely accepted that single-component regular icosahedron with 12 coordination atoms has a space at a center site, to which a smaller atom with 95% radius can rigidly be placed. It is possible that such clusters with a small atom in their center site can have a DRP, leading to the formation of a phase with high GFA.

The local atomic arrangements of the MD–PCM alloy were analyzed using atomic displacements and Voronoi analysis. First, we found that the square root of the mean square displacement ($\sqrt{L_{\text{MSD}}}$) for Zr, Al, and Ni atoms during structural relaxation was as small as the atomic radii of the constituent elements as shown in Fig. 6. The small $\sqrt{L_{\text{MSD}}}$ values indicated that the constituent atoms virtually kept their positions during the structural relaxation in MD–PCM. In other words, the cluster-packed structure was nearly unchanged during the structural relaxation. Thus, it was possible for the alloy created with MD–PCM to keep a

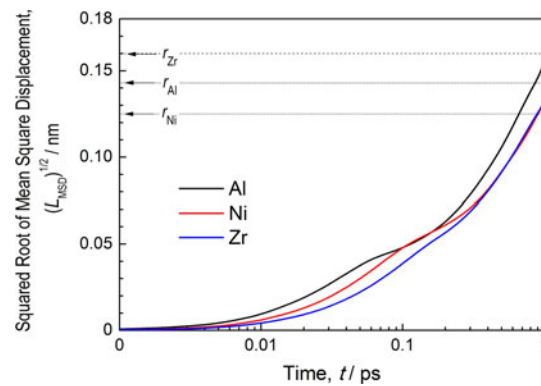


Fig. 6 The square root of mean square displacement ($\sqrt{L_{\text{MSD}}}$) of Zr, Al and Ni atoms during the structural relaxation. The atomic radii of Zr, Al and Ni atoms are also shown for comparison

critically percolated, cluster-packed structure before the structural relaxation.

Voronoi analyses, moreover, revealed that the Ni-centered icosahedral and tetrahedral clusters introduced as initial atomic arrangements are transformed to other types of polyhedra during the structural relaxation. Table 3 shows that Ni atoms tend to form prism-type polyhedra, whereas Zr and Al atoms have a tendency to form icosahedral-type polyhedra. These trends for polyhedra types around Zr, Al and Ni atoms agree with a study by Fukunaga et al. [32], in which Reverse Monte Carlo simulations were performed for $Zr_{60}Al_{15}Ni_{25}$ metallic glass. It should be noted here that the Voronoi analysis in Table 3 explains the formation of icosahedral-type clusters around Zr and Al atoms. This indicates that inter-cluster atomistic rearrangements took place for Zr and Al atoms during the structural relaxation in MD–PCM, since the Zr and Al atoms are coordinated around Ni atoms for the icosahedral and tetrahedral clusters in MD–PCM. Figure 6 and Table 3 reveal the Ni-centered icosahedral and tetrahedral clusters can be appropriate initial atomic arrangements in MD–PCM. They eventually provide local atomic arrangements similar to those of conventional MD simulations in terms of Voronoi analysis.

Conclusions

The $Zr_{0.618}Al_{0.146}Ni_{0.236}$ glassy alloy was created computationally using $Zr_{\phi^{-1}}Al_{\phi^{-4}}Ni_{\phi^{-3}}$ alloy composition ($\phi \sim 1.618$), with local atomic arrangements that consist of icosahedral and tetrahedral clusters with the ratio of number density of $\phi^2:1$. The MD simulations based on the PCM were performed for the alloy through the following two steps. The first step was to create a $Zr_{0.73}Ni_{0.27}$ glassy alloy with conventional MD through a quenching process. The

Table 3 Voronoi Analysis showing the number of polyhedra for the Zr₆₀Al₁₅Ni₂₅ alloy in the liquid, as-quenched (as-Q) and further relaxed (As-Q + Relaxed) states

Polyhedron	Element at center site											
	Zr			Al			Ni					
	Conventional MD		MD-PCM	Conventional MD		MD-PCM	Conventional MD		MD-PCM			
	Liquid	As-Q	As-Q + Relaxed	As-Q + Relaxed	Liquid	As-Q	As-Q + Relaxed	As-Q + Relaxed	Liquid	As-Q	As-Q + Relaxed	As-Q + Relaxed
Trigonal prism	1	2	0	0	4	3	11	7	60	76	90	91
Archimedean prism	10	2	5	0	4	13	20	20	61	62	82	86
Deformed prism	35	29	35	12	34	45	57	61	57	95	72	74
Icosahedron	51	160	142	209	3	23	11	18	0	7	4	1
Deformed icosahedron	231	357	344	332	63	88	76	84	27	12	15	8

The alloys were created by conventional MD simulation from a liquid and MD-PCM with Ni-centered clusters. Liquid phase is a status just before the quenching started in the conventional MD

The Voronoi indices of the five types of polyhedra are: trigonal prism (0 6 0 0) and (0 3 6 0); archimedean prism (0 2 8 0) and (0 4 4 0); deformed prism (0 3 6 1), (0 2 8 1), (0 5 2 0) and (1 3 3 0); icosahedron (0 0 12 0); deformed icosahedron (0 3 6 3), (0 2 8 2), (0 4 4 4), (0 3 6 2), (0 2 8 3), (0 1 10 2), (0 1 10 3), (0 1 10 4) and (0 2 8 4); BCC (0 6 0 8); FCC (0 12 0 0); deformed crystal (0 3 6 4), (0 3 6 5) and (0 4 4 6)

second step was to create a Zr_{0.618}Al_{0.146}Ni_{0.236} alloy from the Zr_{0.73}Ni_{0.27} glassy alloy. In creating the Zr_{0.618}Al_{0.146}Ni_{0.236} alloy with MD-PCM, the replacement of the Zr and Ni atoms in the Zr_{0.73}Ni_{0.27} glassy alloy with the icosahedral and tetrahedral clusters, respectively, was carried out on the basis of the concept of renormalization group in statistical mechanics. Total pair-distribution and interference function analysis revealed that the Zr_{0.618}Al_{0.146}Ni_{0.236} alloy could be formed in a liquid-like state. MD-PCM tended to reproduce conventional MD simulations when the Ni atoms were placed at the center site of the polyhedra. The mean square displacement and Voronoi analysis revealed that the origin of the high GFA of the Zr_{0.618}Al_{0.146}Ni_{0.236} alloy was the critically percolated, cluster-packed structure.

We propose a new method for creating liquid-like structure through MD-PCM that involves clusters, critical concentration for site percolation for a DRP structure, as well as relaxation processes and the renormalization group.

Acknowledgements This work was supported by the Japan Society for the Promotion of Science (JSPS) under grant number 21560715.

References

- Inoue A, Zhang W (2004) Mater Trans 45:584
- Xu D, Lohwongwatana B, Duan G, Johnson WL, Garland C (2004) Acta Mater 52:2621
- Yang L, Xia JH, Wang Q, Dong C, Chen LY, Ou X, Liu JF, Jiang JZ, Klementiev K, Saks K, Franz H, Schneider JR, Gerward L (2006) Appl Phys Lett 88:241913
- Inoue A, Zhang T, Masumoto T (1990) Mater Trans JIM 31:177
- Inoue A, Materials Science Foundations (1998) Bulk amorphous alloys: preparation and fundamental characteristics. Trans Tech Publications, Switzerland
- Inoue A (2000) Acta Mater 48:279
- Yokoyama Y, Mund E, Inoue A, Schultz L (2007) Mater Trans 48:3190
- Zhang QS, Zhang W, Inoue A (2007) Mater Trans 48:629
- Takeuchi A, Yavari AR, Inoue A (2009) Intermetallics 17:696
- Finney JL, Wallage J (1981) J Non-Cryst Solids 43:165
- Fang HZ, Hui X, Chen GL, Öttinger R, Liu YH, Schaefer JA, Liu ZK (2008) Compos Mater Sci 43:1123
- Kelton KF, Gangopadhyay AK, Kim TH, Lee GW (2006) J Non-Cryst Solids 352:5318
- Fitzpatrick JP, Malt RB, Spaepen F (1974) Phys Lett A47:207
- Zallen R (2004) The physics of amorphous solids. Wiley, Weinheim
- Takeuchi A, Yubuta K, Inoue A (2009) 13th International symposium on metastable, amorphous and nanostructured materials. Beijing, China
- Gale WF, Totemeier TC, ASM International (2004) Smithells metals reference book, 8th edn. Elsevier, Oxford
- Sutton D (2002) Platonic and archimedean solids. Walker & Company, New York
- Miracle DB (2004) Nat Mater 3:697
- Miracle DB (2006) Acta Mater 54:4317
- Sheng HW, Luo WK, Alamgir FM, Bai JM, Ma E (2006) Nature 439:419
- Bhatnagar AK, Pan R, Naugle DG (1989) Phys Rev B 39:12460
- Takeuchi A, Yokoyama Y, Kato H, Yubuta K, Inoue A (2009) Intermetallics 16:819
- Gray GW (1974) In: Liquid crystals and plastic crystals, Ellis Horwood series in physical chemistry, vols 1 and 2. Halsted Press, New York
- Sherwood JN (ed) (1979) The plastically crystalline state. Wiley-Interscience Publication, Chichester
- Takeuchi A, Yubuta K, Yokoyama Y, Makino A, Inoue A (2009) Intermetallics 16:283
- Takeuchi A, Yubuta K, Yokoyama Y, Yavari AR, Inoue A (2009) Intermetallics 16:774

27. Mattern N (2007) *J Non-Cryst Solids* 353:1723
28. Debenedetti PG (1996) *Metastable liquids, concepts and principles*. Princeton University Press, New Jersey, USA
29. Rault J (2000) *J Non-Cryst Solids* 271:177
30. Matsubara E, Tamura T, Waseda Y, Inoue A, Zhang T, Masumoto T (1992) *Mater Trans JIM* 33:873
31. Sato S, Sanada T, Saida J, Imafuku M, Matsubara E, Inoue A (2005) *Mater Trans* 46:2893
32. Fukunaga T, Itoh K, Otomo T, Mori K, Sugiyama M, Kato H, Hasegawa M, Hirata A, Hirotsu Y, Hannon AC (2007) *Mater Trans* 48:1698